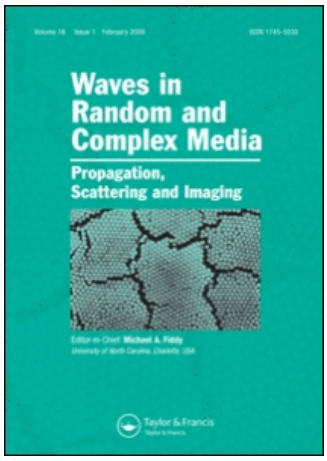

Waves in Random and Complex Media

Publication details, including instructions for authors and subscription information:
http://www-intra.informaworld.com/smpp/title~content=t716100762

Waves and fracture in an inhomogeneous lattice structure

G. S. Mishuris [a]; A. B. Movchan [b]; L. I. Slepyan [c]
[a] Department of Mathematics, Rzeszów University of Technology, Poland
[b] Department of Mathematical Sciences, University of Liverpool,
[c] School of Mechanical Engineering, Tel Aviv University, Israel

Online Publication Date: 01 November 2007
To cite this Article: Mishuris, G. S., Movchan, A. B. and Slepyan, L. I. (2007) 'Waves and fracture in an inhomogeneous lattice structure', Waves in Random and Complex Media, 17:4, 409 - 428
To link to this article: DOI: 10.1080/17455030701459910
URL: http://dx.doi.org/10.1080/17455030701459910

Waves in Random and Complex Media
Vol. 17, No. 4, November 2007, 409–428

Waves and fracture in an inhomogeneous lattice structure

G. S. MISHURIS†, A. B. MOVCHAN‡ and L. I. SLEPYAN§*

†Department of Mathematics, Rzeszów University of Technology, Poland
‡Department of Mathematical Sciences, University of Liverpool
§School of Mechanical Engineering, Tel Aviv University, Israel

(Received 16 February 2007; in final form 1 May 2007)

We analyze a crack propagating in an inhomogeneous rectangular lattice in the state of anti-plane shear. The filtering properties of such a lattice are linked to the energy dissipation due to waves initiated by the crack. The influence of the inhomogeneities within the lattice on the lattice trapping is investigated.

1. Introduction

We consider a square lattice consisting of point particles connected by linearly elastic massless bonds. The lattice layers differ by particle masses so that the cell of periodicity contains three masses. Main features of dynamic fracture are closely connected with the wave characteristics of the body, so that we begin by considering the waves existing in such a lattice.

Waves in periodic structures, in particular, in lattices is a classical topic [1, 2]. It has got the second wind when artificial 'crystals' were revealed as band-gap materials can control the propagation of waves of different nature [3–8]. Within certain limits, a properly designed lattice may control the crack path as artificial crystals (the band-gap materials) can control the propagation of waves of different frequencies and polarization. In the present work, we study for the first time a lattice which is inhomogeneous and stratified.

There is a large, steadily increasing number of papers on fracture in lattices. Numerical simulations of atomic lattices were initiated in [9, 10], and still receive substantial attention in the modern literature (see, for example [11, 12] and references therein). The first analytical solution for a string-like 2D lattice model was obtained in [13]. Similar lattice models were then studied in [14–31]. The main results on this topic are summarized in [32]. Beam-like lattices were studied in [33–40].

There are some essential peculiarities in lattice fracture mechanics. In this model, the crack growth is considered as a consequence of breaks of the bonds, there is no crack edge singularity, and the fracture theory can be based on the classical criteria of the 1D bond strength. In general, there exist dynamic effects even in the case of a slow crack [13, 32]. The discrete

*Corresponding author. E-mail: leonid@eng.tau.ac.il

Waves in Random and Complex Media
ISSN: 1745-5030 (print), 1745-5049 (online)
http://www.tandf.co.uk/journals
DOI: 10.1080/17455030701459910

pulses caused by bond rupture lead to lattice oscillations and to the dynamic amplification factor, which affects the direction of the propagating crack and the crack propagation speed [32, 41]. Due to lattice oscillations, the total energy release rate is a sum of the bond limiting strain energy and the radiation energy rate. From the macrolevel viewpoint, the latter is the dissipation.

The ratio of the bond limiting strain energy to the total fracture energy, and hence the dissipation rate, is represented by a rather complicated non-monotonic function of the crack speed [32, p. 404]. The underlying cause of the wavy behavior of the plot is the dynamic crack-speed-dependent influence of the bond break on the next bond strain [41]. In the above-mentioned analytical studies, uniform periodic lattices were always considered. We now study how the lattice inhomogeneity influences the dissipation. In this study, the masses at the lattice junctions are assumed to be different. A 2D rectangular lattice for mode III fracture is considered. First we derive dispersion relations for the waves in the undamaged lattice. Then the problem is considered for the lattice with a semi-infinite straight crack propagating at a subcritical constant speed. This also includes the case of an orthotropic lattice.

2. The lattice

We consider a 2D rectangular lattice shown in figure 1a. The particles shown as black (white) discs are assumed to have mass m_1 (m_2). The system is normalized in such a way that the stiffness of the bonds connecting neighboring particles, the lattice spacing and the averaged density are chosen as natural units. Therefore, the average density is $(2m_1 + m_2)/3 = 1$, and the low-frequency wave speed is equal to $c = 1$.

We consider the dynamic state of anti-plane shear corresponding to transverse oscillation of the particles within the lattice. The equations of motion are written for three particles within the elementary cell of the periodic structure shown in figure 1(b). The displacement is denoted as $u_{j,m,n}$, where (m, n), $m, n = 0, \pm1, \pm2, \ldots$, stands for the multi-index characterizing the position of the cell $m\boldsymbol{e}^{(1)} + 3n\boldsymbol{e}^{(2)}$, whereas $j = 0, 1, 2$ is the index characterizing the particle

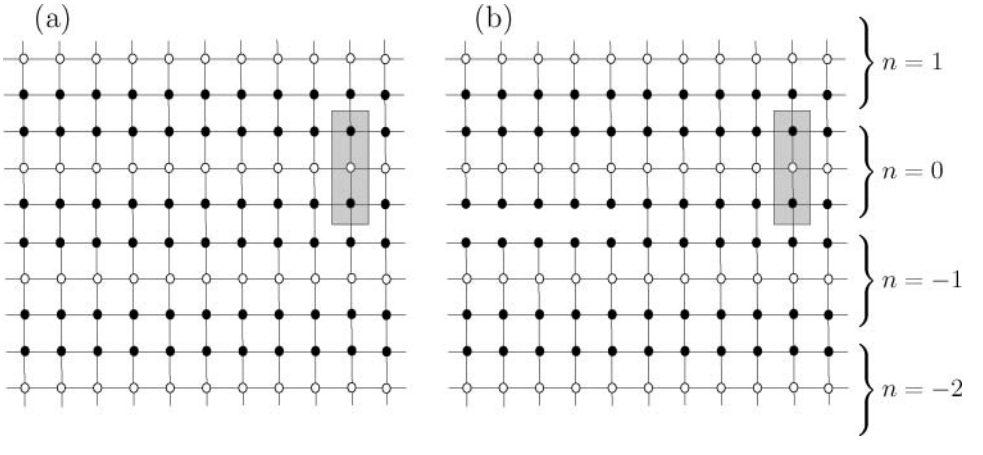

Figure 1. Inhomogeneous lattice structures: (a) Undamaged lattice; (b) lattice with a crack. The 'white'-to-'black' mass ratio is denoted by μ. The elementary cell is shown as a shaded rectangle. The horizontal and vertical coordinates of the cell are denoted by m and n, respectively.

within the cell. The equations of motion of the intact lattice have the form:

$$\begin{aligned}
\frac{3}{2+\mu}\ddot{u}_{0,m,n} &= u_{0,m-1,n} + u_{0,m+1,n} + u_{1,m,n} + u_{2,m,n-1} - 4u_{0,m,n},\\
\frac{3\mu}{2+\mu}\ddot{u}_{1,m,n} &= u_{1,m-1,n} + u_{1,m+1,n} + u_{2,m,n} + u_{0,m,n} - 4u_{1,m,n},\\
\frac{3}{2+\mu}\ddot{u}_{2,m,n} &= u_{2,m-1,n} + u_{2,m+1,n} + u_{0,m,n+1} + u_{1,m,n} - 4u_{2,m,n},
\end{aligned} \tag{1}$$

where $\mu = m_2/m_1$. Note that when a crack is introduced the equations for the crack-face particles are changed, as described in section 4.

3. Waves in the undamaged lattice

3.1 *Dispersion relations*

Sinusoidal waves are sought in the form:

$$u_{j,m,n} = U_j \mathrm{e}^{\mathrm{i}(\omega t - k_x m - 3k_y n)}, \tag{2}$$

where U_j, $j = 0, 1, 2$, are the amplitudes, ω is the radian frequency, and (k_x, k_y) is the wavevector. Note that, in the k_x, k_y-plane, the cell of periodicity is $(-\pi, \pi] \times (-\pi/3, \pi/3]$. The periodic pattern corresponds to the Floquet representation of eigensolutions within an elementary cell consisting of three particles.

The system (1) yields

$$\begin{aligned}
S_2 U_0 - U_1 - U_2 \mathrm{e}^{3\mathrm{i}k_y} &= 0,\\
S_1 U_1 - U_2 - U_0 &= 0,\\
S_2 U_2 - U_0 \mathrm{e}^{-3\mathrm{i}k_y} - U_1 &= 0,
\end{aligned} \tag{3}$$

where

$$S_1 = 4 - 2\cos k_x - \frac{3\mu}{2+\mu}\omega^2, \quad S_2 = 4 - 2\cos k_x - \frac{3}{2+\mu}\omega^2. \tag{4}$$

This system of linear algebraic equations with respect to U_0, U_1, U_2 has a nontrivial solution if and only if

$$\begin{aligned}
\mathcal{D} &= \det \begin{pmatrix} S_2 & -1 & -\mathrm{e}^{3\mathrm{i}k_y} \\ -1 & S_1 & -1 \\ -\mathrm{e}^{-3\mathrm{i}k_y} & -1 & S_2 \end{pmatrix}\\
&= S_1\left(S_2^2 - 1\right) - 2S_2 - 2\cos(3k_y)\\
&= -\frac{27\mu}{(2+\mu)^3}\omega^6 + \frac{18(2\mu+1)}{(2+\mu)^2}(2-\cos k_x)\omega^4 - 3\alpha\omega^2 + \beta = 0,
\end{aligned} \tag{5}$$

where

$$\alpha = 4(2-\cos k_x)^2 - 1, \quad \beta = 8(2-\cos k_x)^3 - 6(2-\cos k_x) - 2\cos(3k_y). \tag{6}$$

This bicubic dispersion equation allows for explicit closed form solutions, but it appears too cumbersome to be written down here. The dispersion surfaces representing the solutions $\omega_j(k_x, k_y)$ of the dispersion equation (5) are shown in figure 2. Furthermore, in figures 3 and 4

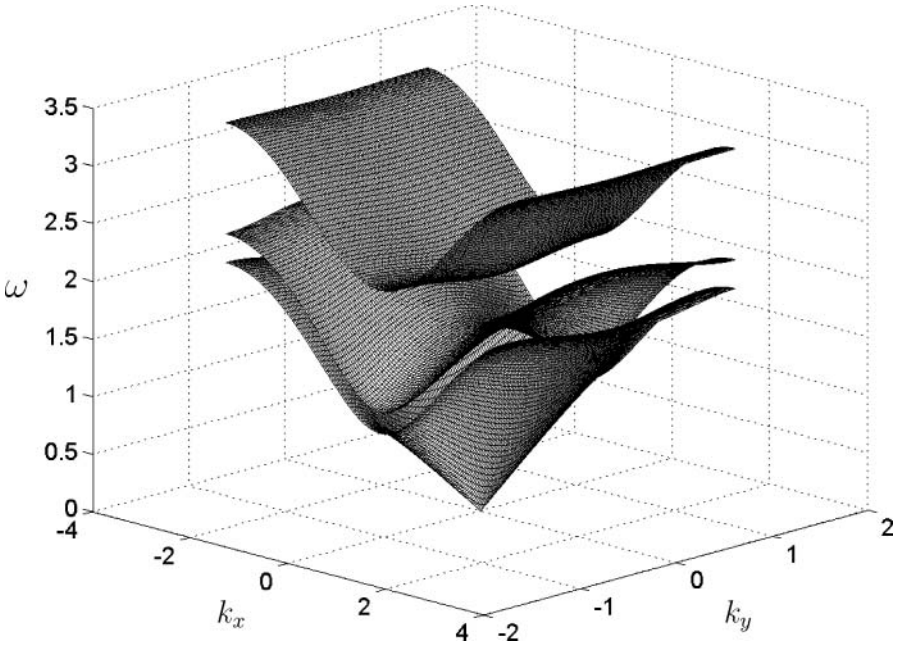

Figure 2. The three-branch dispersion diagram for $\mu = 0.5$.

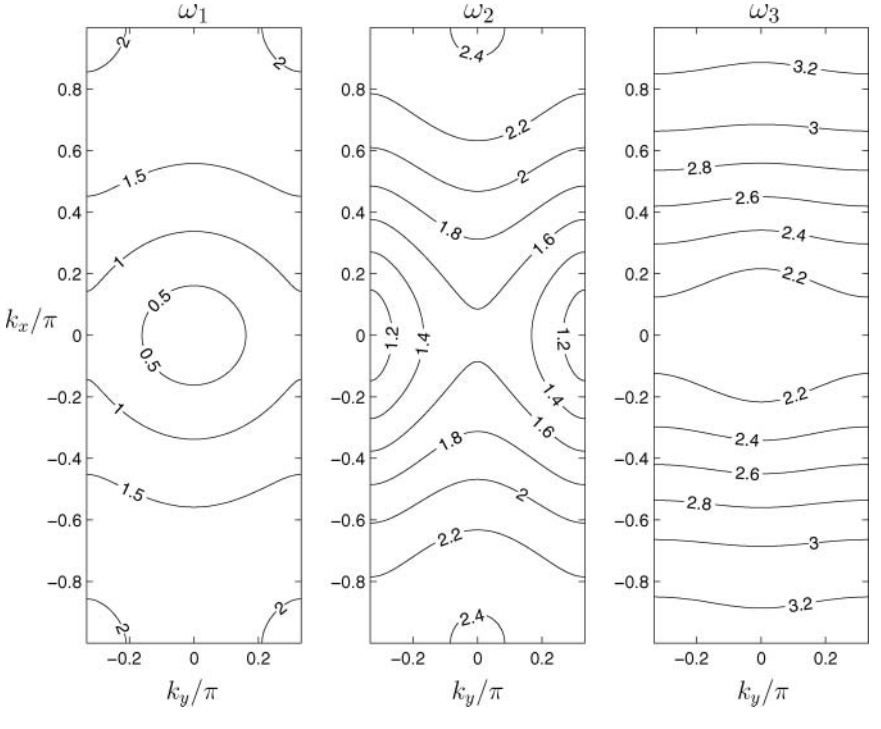

Figure 3. Contour line plots for three dispersion branches for $\mu = 0.5$.

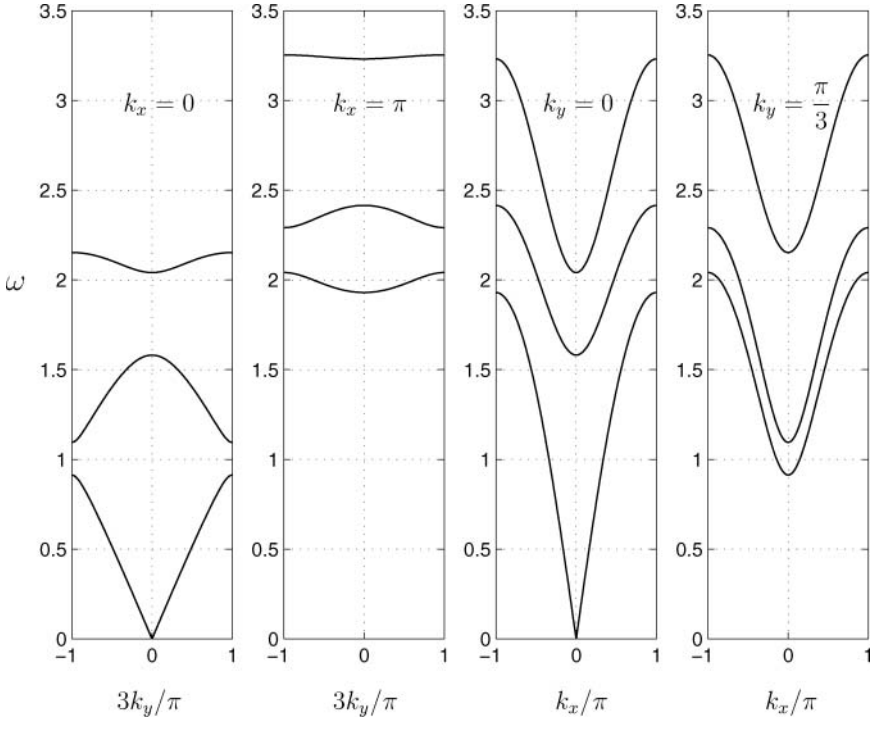

Figure 4. Dispersion curves representing different cross-sections of the dispersion surfaces for $\mu = 0.5$.

we give the contourline plots for the dispersion surfaces and the vertical cross-sections of these surfaces for $\mu = 0.5$. In particular, the dispersion diagrams in figures 4(c) and 4(d) correspond to waves excited by the propagating crack and will be discussed further in the sequel of the paper.

For long waves ($k_x, k_y \to 0$), the results are consistent with the corresponding asymptote for the homogeneous lattice:

$$\omega^2 \sim k_x^2 + k_y^2. \tag{7}$$

Note that for $\mu \neq 1$ there exist three different branches of the dispersion relation.

3.2 *Uniform lattice*

In this case, $\mu = 1$, the three-branch relation is a consequence of the representation of the cell of periodicity as the 1×3 rectangle. The condition $k_x, k_y \to 0$ implies that the state in the neighboring rectangular cells is asymptotically the same, but particles within the cell may oscillate. Thus, two additional branches for solutions of the dispersion equation occur here.

All three branches are defined by the equation

$$S^3 - 3S - 2\cos 3k_y = 0. \tag{8}$$

(Compare with (5), with $S_1 = S_2 = S$.) The roots follow as

$$S^{(1)} = 2\cos k_y\,, \quad S^{(2,3)} = -2\cos(k_y + \pi/3),$$

and correspondingly

$$\omega_1^2(1, k_x, k_y) = 4 - 2\cos k_x - 2\cos k_y,$$
$$\omega_{2,3}^2(1, k_x, k_y) = 4 - 2\cos k_x + 2\cos(k_y + \pi/3). \tag{9}$$

The first (acoustic) branch has a conical point at the origin ($k_x = k_y = 0$):

$$\omega_1 \sim \sqrt{k_x^2 + k_y^2} \text{ as } k_x^2 + k_y^2 \to 0. \tag{10}$$

We note that this relation is valid for any μ (see (7)). For a general choice of μ, we have

$$\omega_1(\mu, 0, 0) = 0, \quad \omega_2^2(\mu, 0, 0) = 2 + \mu\,, \quad \omega_3^2(\mu, 0, 0) = \frac{(2+\mu)^2}{3\mu}. \tag{11}$$

3.3 *Asymptotic approximations of eigenfrequencies for high-contrast lattices*

Asymptotically, when $\mu \to 0$ the solutions of the dispersion equation take the form

$$\omega_{1,2}^2(\mu, k_x, k_y) \to \frac{\alpha \mp \sqrt{\alpha^2 - 2\beta(2 - \cos k_x)}}{3(2 - \cos k_x)},$$
$$\omega_3^2(\mu, k_x, k_y) \sim \frac{4(2 - \cos k_x)}{3\mu}, \tag{12}$$

while in the opposite case, $\mu \to \infty$, we have

$$\omega_1^2(\mu, k_x, k_y) \to \beta/(3\alpha),$$
$$\omega_2^2(\mu, k_x, k_y) \sim (\mu/3)(5 - 2\cos k_x), \quad \omega_3^2(\mu, k_x, k_y) \sim (\mu/3)(3 - 2\cos k_x), \tag{13}$$

where the quantities α and β are defined in (6). It follows that, in the cases of high-contrast lattices, there are band gaps in ω where no propagating wave exists. Furthermore, when the 'black' masses (see figure 1a) vanish, as $\mu \to \infty$, only the first branch (for ω_1) remains.

3.4 *Two special cases*

In the special cases, $k_y = 0$ and $k_y = \pi/3$, the dispersion relations (5) can be simplified. Namely, for $k_y = 0$ we have $\cos 3k_y = 1$, and for $k_y = \pi/3$ we observe that $\cos 3k_y = -1$, so that one of the roots can be written in the form

$$\omega^2 = \omega_3^2 = \frac{2+\mu}{3}(5 - 2\cos k) \quad (k_y = 0),$$
$$\omega^2 = \omega_3^2 = \frac{2+\mu}{3}(3 - 2\cos k) \quad (k_y = \pi/3), \tag{14}$$

where the notation $k_x = k$ is used. The other roots are elementary and defined by the corresponding quadratic equations. For $k_y = 0$ they are

$$\omega_{1,2}^2(\mu, k, 0) = \frac{2+\mu}{6\mu}[P_+(\mu, k) \mp \sqrt{Q_+(\mu, k)}] \tag{15}$$

with

$$P_+(\mu, k) = 3\mu + 4 - 2(1+\mu)\cos k,$$
$$Q_+(\mu, k) = 9\mu^2 - 16\mu + 16 - (16 - 28\mu + 12\mu^2)\cos k + 4(1-\mu)^2\cos^2 k, \tag{16}$$

and for $k_y = \pi/3$

$$\omega_{1,2}^2(\mu, k, \pm\pi/3) = \frac{2+\mu}{6\mu}[P_-(\mu, k) \mp \sqrt{Q_-(\mu, k)}], \tag{17}$$

with

$$P_-(\mu, k) = 5\mu + 4 - 2(1+\mu)\cos k,$$
$$Q_-(\mu, k) = 25\mu^2 - 32\mu + 16 - (16 - 36\mu + 20\mu^2)\cos k + 4(1-\mu)^2\cos^2 k. \tag{18}$$

The corresponding dispersion diagrams, for the case of $\mu = 0.5$, are shown in figures 4(c) and 4(d).

In the dynamic fracture problem considered below, the propagating crack excites some of these waves, and therefore creates a speed-dependent dissipation.

4. Lattice with a propagating crack

4.1 *The Wiener–Hopf problem*

We now introduce a semi-infinite crack, $m < vt, t > -\infty$, propagating along a line between the layers $(0, m, 0)$ and $(2, m, -1)$, as shown in figure 1(b), with a constant speed, $v > 0$. The 'steady state' formulation is adopted, and it is assumed that the displacement $u_{j,m,n}(t)$ depends only on the variables j, $\eta = m - vt$ and n. The crack propagation is considered as a consequence of the bond breakage along the above-mentioned line at $\eta = 0$ (i.e. $t = m/v$). We may thus describe the dynamic field by means of functions $u_{j,n}(\eta)$. In accordance with the mode III symmetry

$$u_{0,n}(\eta) = -u_{2,-n-1}(\eta), \quad u_{1,n}(\eta) = -u_{1,-n-1}(\eta), \quad u_{2,n}(\eta) = -u_{0,-n-1}(\eta). \tag{19}$$

In terms of the Fourier transform $u_{j,n}^F(k)$ of $u_{j,n}(\eta)$ with respect to η (considered as a continuous variable for any m), the equations for the undamaged lattice (see (1)) become

$$\begin{aligned} \mathcal{S}_2 u_{0,n}^F - u_{1,n}^F - u_{2,n-1}^F &= 0, \\ \mathcal{S}_1 u_{1,n}^F - u_{0,n}^F - u_{2,n}^F &= 0, \\ \mathcal{S}_2 u_{2,n}^F - u_{0,n+1}^F - u_{1,n}^F &= 0, \end{aligned} \tag{20}$$

with

$$\mathcal{S}_1(k) = 4 - 2\cos k + \frac{3\mu}{2+\mu}(0 + ikv)^2, \quad \mathcal{S}_2(k) = 4 - 2\cos k + \frac{3}{2+\mu}(0 + ikv)^2, \tag{21}$$

where

$$(0 + ikv) = \lim_{\varepsilon \to +0}(\varepsilon + ikv), \tag{22}$$

which follows from the causality principle for steady-state solutions [32]. The latter relation allows us to choose the correct integration path in the evaluation of the inverse transform to avoid crossing the singular points. (For $\Re\varepsilon > 0$ the considered functions have no singular points on the real k-axis.)

For the lattice with the crack, equations (20) are valid for $n > 0$ and for $n < -1$. For the upper half-plane we use the representation

$$u_{j,n}^F(k) = u_j^F(k)\lambda^n(k), \quad u_j^F = u_{j,0}^F, \quad |\lambda| \leq 1. \tag{23}$$

For $n > 0$ equations (20) become

$$\begin{aligned} \mathcal{S}_2 u_0^F - u_1^F - u_2^F/\lambda = 0, \\ \mathcal{S}_1 u_1^F - u_0^F - u_2^F = 0, \\ \mathcal{S}_2 u_2^F - \lambda u_0^F - u_1^F = 0. \end{aligned} \tag{24}$$

The linear algebraic system (24) has a nontrivial solution if and only if

$$\det \begin{pmatrix} \mathcal{S}_2 & -1 & -\lambda^{-1} \\ -1 & \mathcal{S}_1 & -1 \\ -\lambda & -1 & \mathcal{S}_2 \end{pmatrix} = 0. \tag{25}$$

It follows that

$$\lambda = P - \sqrt{P^2 - 1}, \quad P = \frac{1}{2}\big(\mathcal{S}_1 \mathcal{S}_2^2 - 2\mathcal{S}_2 - \mathcal{S}_1\big). \tag{26}$$

In this relation, if $\varepsilon = 0$ then P is a real-valued function of the real variable k; it is a complex-valued function otherwise. At the same time the function in (26) maps the complex plane P with the $(-1, 1)$ branch cut into a unit circle or its exterior in the λ-plane, depending on the branch of the square root function (the inverse function, $P = (1/2)(\lambda + 1/\lambda)$, is known as the Zhukovskii function). Thus the relation in (22) and the condition $|\lambda| \le 1$ result in the following choice for the square root branch in (26):

$$\begin{aligned} &\sqrt{P^2 - 1} > 0 \quad (P > 1), \quad \sqrt{P^2 - 1} < 0 \quad (P < -1), \\ &\sqrt{P^2 - 1} = \mathrm{i}\sqrt{1 - P^2}\,\operatorname{sign} k \quad [\lambda = P = 1 \ \text{ as } \ k = 0]. \end{aligned} \tag{27}$$

It can be seen that the functions $S_{1,2}$ and $\mathcal{S}_{1,2}$ and equations (5) and (25) coincide if we take

$$\omega = kv \quad \text{and} \quad k_y = (1/3)\mathrm{i} \ln \lambda(k) \quad (k = k_x). \tag{28}$$

So the intersection of the plane $\omega = k_x v$ with the dispersion surfaces considered in section 3 and the last equality in (28) define the waves which can be excited by the propagating crack. Note that $|\lambda| = 1$ and $|\lambda| < 1$ correspond to sinusoidal and exponentially decreasing waves, respectively. By solving the problem, we obtain more specific information about the waves excited by the crack and also obtain the total dissipation as a function of the crack speed.

We now turn to the equation for particle displacements $u_{0,0}(\eta)$ on the crack face, and note that $u_{2,-1}(\eta) = -u_{0,0}(\eta)$. Let us use the representations

$$u_{0,0}^F(k) = u_+(k) + u_-(k), \quad u_\pm(k) = \big[u_{0,0}(\eta) H(\pm\eta)\big]^F, \tag{29}$$

where H is the Heaviside unit step function. Let σ denote the traction on the boundary of the upper half-plane. It is assumed that the crack faces are traction free, i.e. for $\eta < 0$ we have

$$\sigma(\eta) = 0\,, \quad \sigma_- = 0, \tag{30}$$

whereas for $\eta > 0$

$$\sigma(\eta) = 2u_{0,0}(\eta)\,, \quad \sigma_+ = 2u_+. \tag{31}$$

Accordingly, we modify the first equation in the system (24). Using the relations

$$(\mathcal{S}_1 \mathcal{S}_2 - 1) u_1^F = (\mathcal{S}_2 + \lambda) u_0^F \tag{32}$$

and

$$\sigma_+ = u_1^F - (\mathcal{S}_2 - 1) u_0^F \tag{33}$$

we arrive at the functional equation of the Wiener–Hopf type for the functions $u_{\pm}(k)$

$$\mathcal{Q}_1(k)u_+(k) + \mathcal{Q}_2(k)u_-(k) = 0,$$

$$\mathcal{Q}_1(k) = \mathcal{S}_2 + 1 - \frac{\mathcal{S}_2 + \lambda}{\mathcal{S}_1\mathcal{S}_2 - 1}, \quad \mathcal{Q}_2(k) = \mathcal{S}_2 - 1 - \frac{\mathcal{S}_2 + \lambda}{\mathcal{S}_1\mathcal{S}_2 - 1}, \quad (34)$$

where $\mathcal{S}_{1,2}$ and λ are defined by equations (21) and (26), respectively.

4.2 *Dissipative waves*

A nonzero singular point of $u_+(k)$ or $u_-(k)$ defining a high-frequency propagating wave originates from a zero point of $\mathcal{Q}_1(k)$ or $\mathcal{Q}_2(k)$ (see (34)). The first roots of the equations

$$\mathcal{Q}_1(k) = 0 \quad \text{and} \quad \mathcal{Q}_2(k) = 0 \quad (35)$$

for $\mu \neq 1$ can be easily found from the equations

$$\mathcal{S}_2 = \mp 1, \quad (36)$$

which correspond to

$$\lambda = \pm 1,$$

respectively (see (21) and (26)). It follows that

$$\mathcal{Q}_1 = 0: \quad \omega^2 = (kv)^2 = \frac{2+\mu}{3}(5 - 2\cos k), \quad \lambda = 1 \quad (k_y = 0),$$

$$\mathcal{Q}_2 = 0: \quad \omega^2 = (kv)^2 = \frac{2+\mu}{3}(3 - 2\cos k), \quad \lambda = -1 \quad (k_y = \pi/3). \quad (37)$$

These dispersion relations coincide with those presented in (14). The other frequencies also correspond to these values of k_y considered in section 3, namely,

$$\mathcal{Q}_1 = 0: \quad \omega^2 = \omega_{1,2}^2, \quad \lambda = -1 \quad (k_y = \pi/3), \quad (38)$$

where $\omega_{1,2}$ are defined in (17), and

$$\mathcal{Q}_2 = 0: \quad \omega^2 = \omega_{1,2}^2, \quad \lambda = 1 \quad (k_y = 0), \quad (39)$$

where $\omega_{1,2}$ are defined in (15). Note that each of the functions $\mathcal{Q}_{1,2}$ has zeros corresponding to both values of k_y: 0 ($\lambda = 1$) and $\pi/3$ ($\lambda = -1$). For the homogeneous lattice, $\mu = 1$

$$\mathcal{S}_1 = \mathcal{S}_2 = \mathcal{S} = \pm 2,$$

$$\mathcal{S} = -2: \quad \omega^2 = 6 - 2\cos k, \quad \lambda = -1 \quad (\mathcal{Q}_1 = 0),$$

$$\mathcal{S} = 2: \quad \omega^2 = 2 - 2\cos k, \quad \lambda = 1 \quad (\mathcal{Q}_2 = 0) \quad (40)$$

just as expected [compare with relations (11.6) and (11.105)–(11.107) in [32]].

We now show that, in the dissipative waves corresponding $\lambda = \pm 1$, there is no averaged energy flux in the y-direction. Let us consider the energy flux from the node $(2, n)$ to the node $(0, n+1)$. Taking an average over the corresponding time period we can write

$$N_y = \frac{1}{2}\Im[\omega\lambda u_0\overline{(u_2 - \lambda u_0)}], \quad (41)$$

where $\lambda u_{0,n} = u_{0,n+1}$. The considered waves satisfy the system of equations (3) with $\mathrm{e}^{-3\mathrm{i}k_y} = \lambda = \pm 1$. Besides, ω and $S_{1,2}$ are real. It follows that the product in the square brackets is real,

and hence

$$N_y = 0. \tag{42}$$

Thus, the y-component of the group velocity of these waves is equal to zero. Consequently, these dissipative waves propagate mainly parallel to the crack. However, oscillations percolate in the y-direction, and this explains why the steady-state wave field is not localized at the crack line. A root of the equation $\omega(k) = k_x v$, where v is the phase velocity of the wave equal to the crack speed, defines the wavenumber k_x. For $v > 0$, there is a finite number of roots, increasing to infinity as v tends to zero. On the crack-face line the wave is placed ahead of the crack if the group velocity exceeds the crack speed, and it is behind the crack edge otherwise. Other dissipative waves (the waves corresponding to complex λ) can be found using the stationary phase method in the inverse Fourier transform assuming both variables, η and n, tend to infinity.

4.3 *Factorization and solution of the Wiener–Hopf problem*

We now introduce the quantity

$$L(k) = \mathcal{Q}_1/\mathcal{Q}_2 \tag{43}$$

as the kernel of the Wiener–Hopf equation written in the form

$$L(k)u_+(k) + u_-(k) = 0. \tag{44}$$

According to the Index Theorem [32, p. 451], the index of $L(k)$ is equal to zero, and if $\mu < \infty$ (implying that every lattice junction adjacent to the crack has a non-zero mass) then $L(\pm\infty) = 1$. The factorization is standard:

$$\begin{aligned} L(k) &= L_+(k)L_-(k), \\ L_\pm(k) &= \exp\left[\pm \frac{1}{2\pi \mathrm{i}} \int_{-\infty}^{\infty} \frac{\ln L(\xi)}{\xi - k}\, \mathrm{d}\xi \right], \end{aligned} \tag{45}$$

where $\Im k > 0$ for L_+ and $\Im k < 0$ for L_-. Recall that there are no singularities on the integration path if $\varepsilon > 0$, and the definition $(0 + \mathrm{i}kv)$ is used as the limit from above (see (22)).

The equation (44) takes the form

$$L_+(k)u_+(k) + L_-^{-1}u_-(k) = 0. \tag{46}$$

The causality principle adopted here leads to the conclusion that the homogeneous equation (46) only admits the trivial solution. To allow for a contribution from remote external forces, we introduce the δ-function term in the right-hand side of (46) (see [32], Chapter 14). Thus, the modified equation can be written in the form

$$L_+(k)u_+(k) + L_-^{-1}u_-(k) = C[(0 + \mathrm{i}k)^{-1} + (0 - \mathrm{i}k)^{-1}], \tag{47}$$

where C is a constant. In terms of the Fourier transform, the solution is obtained as follows

$$u_+(k) = \frac{C}{(0 - \mathrm{i}k)L_+(k)}, \quad u_-(k) = \frac{CL_-(k)}{0 + \mathrm{i}k}. \tag{48}$$

This is the only solution satisfying the regularity condition including the boundedness of the displacements at the crack edge. The singular point $k = 0$ ($\varepsilon = +0$) defines the long wave carrying energy to the propagating crack from $-\infty$ (this wave corresponds to that in the homogenized medium with the moving crack), whereas the real singular points of $L_\pm(k)$ and zeros of $L_+(k)$ correspond to the high-frequency waves excited by the propagating crack.

4.4 *Local and global energy release rates*

Let G_0 and G be the local energy release rate for the lattice and the global energy release rate for the corresponding homogenized medium, respectively. In other words, G_0 is the strain energy accumulated in the bond before it breaks, whereas G is the energy release rate corresponding to the long-wave (low-frequency) asymptote of the exact lattice solution. In the homogeneous problem considered here, the latter is the macrolevel energy flux from the infinity. The difference, $G - G_0$, represents the energy of high-frequency waves radiated by the propagating crack; from the macrolevel viewpoint this is dissipation.

The limiting elongation of the bond is equal to $2u(\eta)$ at $\eta = 0$, and

$$2u(0) = 2 \lim_{k \to \mathrm{i}\infty} (-\mathrm{i}k) u_+(k) = 2C, \quad [\text{we recall that } \lim_{k \to \mathrm{i}\infty} L_+(k) = 1] \tag{49}$$

and hence, in our solution, the limiting energy of the linearly elastic bond is given by

$$G_0 = 2C^2. \tag{50}$$

At the same time, the long-wave asymptotes ($k \to 0$) of σ_+ and u_- are defined by the same formulas as for the homogeneous lattice [32, Section 11.5.2, $a = 1$, $\mu = 1$, $A_0 = C$]

$$\sigma_+(k) \sim \frac{\sqrt{2}C(1 - v^2)^{1/4}}{\mathcal{R}(v)\sqrt{0 - \mathrm{i}k}},$$

$$u_-(k) \sim \frac{\sqrt{2}C}{(1 - v^2)^{1/4}\mathcal{R}(v)(0 + \mathrm{i}k)^{3/2}}, \tag{51}$$

with

$$\mathcal{R}(v) = \exp\left[\frac{1}{\pi}\int_0^\infty \frac{\operatorname{Arg} L(k)}{k}\,\mathrm{d}k\right], \tag{52}$$

where $\operatorname{Arg} L(k)$ depends on the lattice structure (in our case, it depends on the mass ratio, μ).

Based on formulae (48) and [32, equation (1.42), p. 27], we can represent the global energy release in the form

$$G = \lim_{\varepsilon \to +0} \frac{2C^2 L_-(-\mathrm{i}\varepsilon)}{L_+(\mathrm{i}\varepsilon)} = \frac{2C^2}{\mathcal{R}^2(v)}. \tag{53}$$

Note that $\operatorname{Arg} L(k)$ is a function with a compact support (for $v > 0$) increasing with the decrease of v. As an example, the argument $\operatorname{Arg} L(k)$ is plotted in figure 5 for $\mu = 0.5$ and $v = 0.2$, where the dashed curves correspond to a small $\varepsilon = 0.001$ (see relation (22)), whereas the solid lines correspond to the limit, $\varepsilon = +0$.

In connection with the calculation of the energy ratio, we note that the functions $\mathcal{Q}_1(k)$ and $\mathcal{Q}_2(k)$ have square-root type zeros, and these are the only points where the piecewise constant argument, $\operatorname{Arg} L(k)$, changes. In particular, when the function $P(k)$ (see (26)) varies in the interval $-1 < P < 1$, it appears that $\Re L(k) \equiv 0$ and $\operatorname{Arg} L(k)$ does not change. At the end points of this interval, $P = -1$ or $P = 1$, one of the functions $\mathcal{Q}_{1,2}$ is equal to zero.

According to (22), as the increasing parameter k crosses a zero point $k = k_v$, the argument of $L(k)$ takes a jump $\delta\mathrm{Arg}$ determined as follows:

$$\delta\mathrm{Arg} = \frac{\pi}{2} \quad (\mathcal{Q}_1 = 0\,,\, v > v_g \quad \text{or} \quad \mathcal{Q}_2 = 0\,,\, v < v_g)\,,$$

$$\delta\mathrm{Arg} = -\frac{\pi}{2} \quad (\mathcal{Q}_1 = 0\,,\, v < v_g \quad \text{or} \quad \mathcal{Q}_2 = 0\,,\, v > v_g), \tag{54}$$

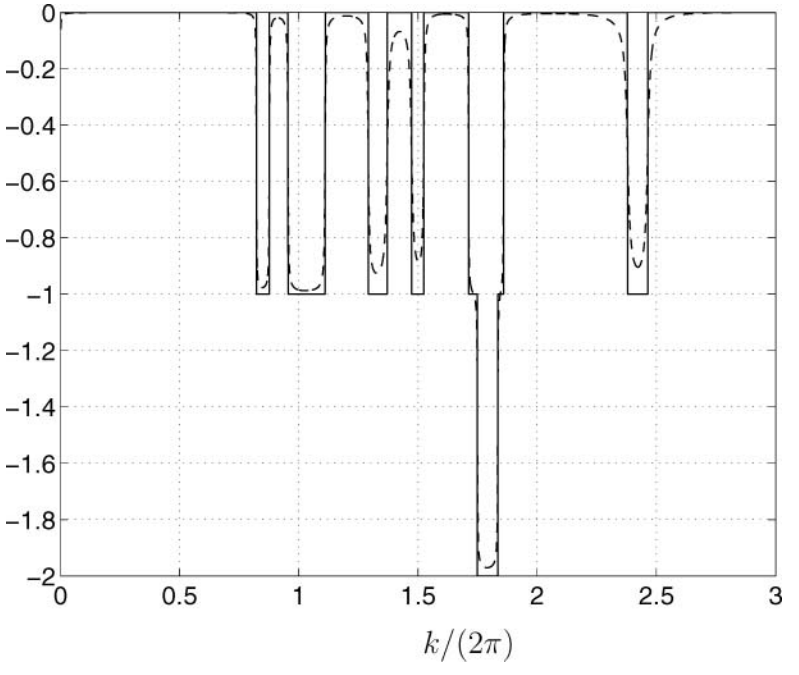

Figure 5. The normalized argument $2\pi^{-1}\mathrm{Arg}L(k)$ calculated for $\mu = 0.5$ and $v = 0.2$ with $\varepsilon = 0.001$ (dashed line) and $\varepsilon = +0$ (solid line).

where $v_g = \mathrm{d}\omega/\mathrm{d}k$ is the group velocity corresponding to wavenumber k_ν of the considered (crossed) wave mode. In figures 6 and 8, the dispersion relations corresponding to the equality $\mathcal{Q}_1 = 0$ are shown by dashed curves, whereas the solid curves correspond to the equality $\mathcal{Q}_2 = 0$. Thus, the rule (54) allows one to extract the argument distribution based on the dispersion diagram combined with the kv-rays.

Taking into account the fact that the argument is a piecewise-constant function of k formed in accordance with the rule (54), the formula (52) can be represented in terms of the zeros of $\mathcal{Q}_1(k)$ and $\mathcal{Q}_2(k)$ as follows:

$$\mathcal{R}(v) = \left(\prod_\nu \frac{k_{1,\nu}^- k_{2,\nu}^+}{k_{1,\nu}^+ k_{2,\nu}^-} \right)^{1/2}, \tag{55}$$

where $k_{1(2),\nu}^{\pm}$ are zeros of $\mathcal{Q}_{1(2)}$, respectively; the superscripts '+' and '−' correspond to the inequalities $v > v_g$ and $v < v_g$, respectively. The product incorporates all the zeros corresponding to a given crack speed v.

Finally, the energy ratio becomes

$$\frac{G_0}{G} = \mathcal{R}^2(v) = \prod_\nu \frac{k_{1,\nu}^- k_{2,\nu}^+}{k_{1,\nu}^+ k_{2,\nu}^-}. \tag{56}$$

The diagrams (for the case of $\mu = 0.5$) including the dispersion curves, intersecting with the rays $\omega = kv$ for certain fixed values of the crack speed v, as well as the corresponding diagrams for $\mathrm{Arg}\, L(k)$ are presented in figures 6(a) and 6(b), respectively. For the hypothetical supercritical crack speed $v = 1.5$ it can be seen that $\mathrm{Arg}\, L(k)$ is nonzero beginning from $k = 0$, and the integral in (52) does not exist. Physically this means that supercritical crack speeds,

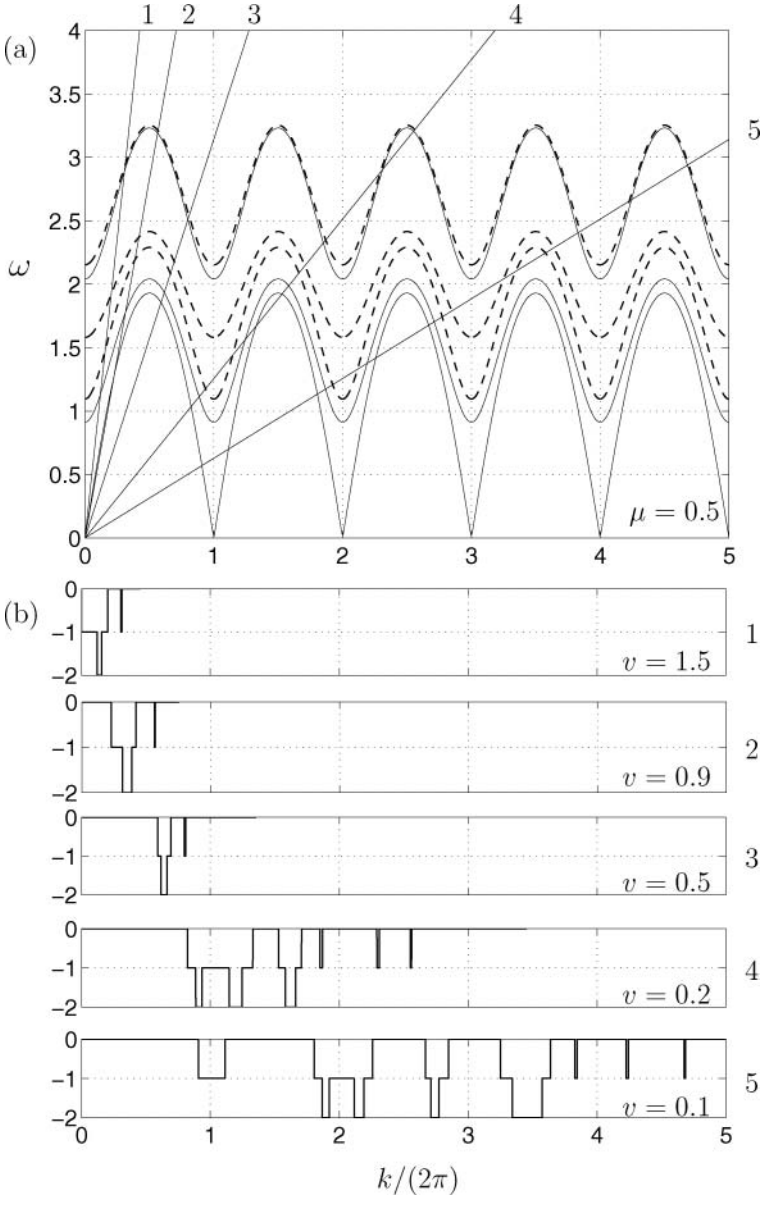

Figure 6. (a) Dispersion diagrams together with the rays $\omega = kv$. (b) The corresponding normalized argument $2\pi^{-1}\mathrm{Arg}L(k)$ for $\mu = 0.5$. The rays numbers, $j = 1, 2, \ldots, 5$, on the dispersion diagram (a) are repeated on the argument diagrams (b). Here and in the following figures, the dashed dispersion curves correspond to zeros of $\mathcal{Q}_1(k)$, whereas the solid curves correspond to zeros of $\mathcal{Q}_2(k)$.

$v > 1$, are forbidden. (The nonzero region of the argument moves to the origin, $k = 0$, as the crack speed tends to the critical value from below, and the integral in (52) tends to minus infinity. Thus $\mathcal{R} \to 0$, which implies that the crack resistance tends to infinity.)

The results of calculations of the energy ratio, $\mathcal{R}^2(v)$, for a number of values of the lattice contrast μ, are presented in figure 7. In figure 8, we also present the dispersion diagrams together with the rays $\omega = kv$ for $v = 0.1$, 0.2, 0.5 and 0.9.

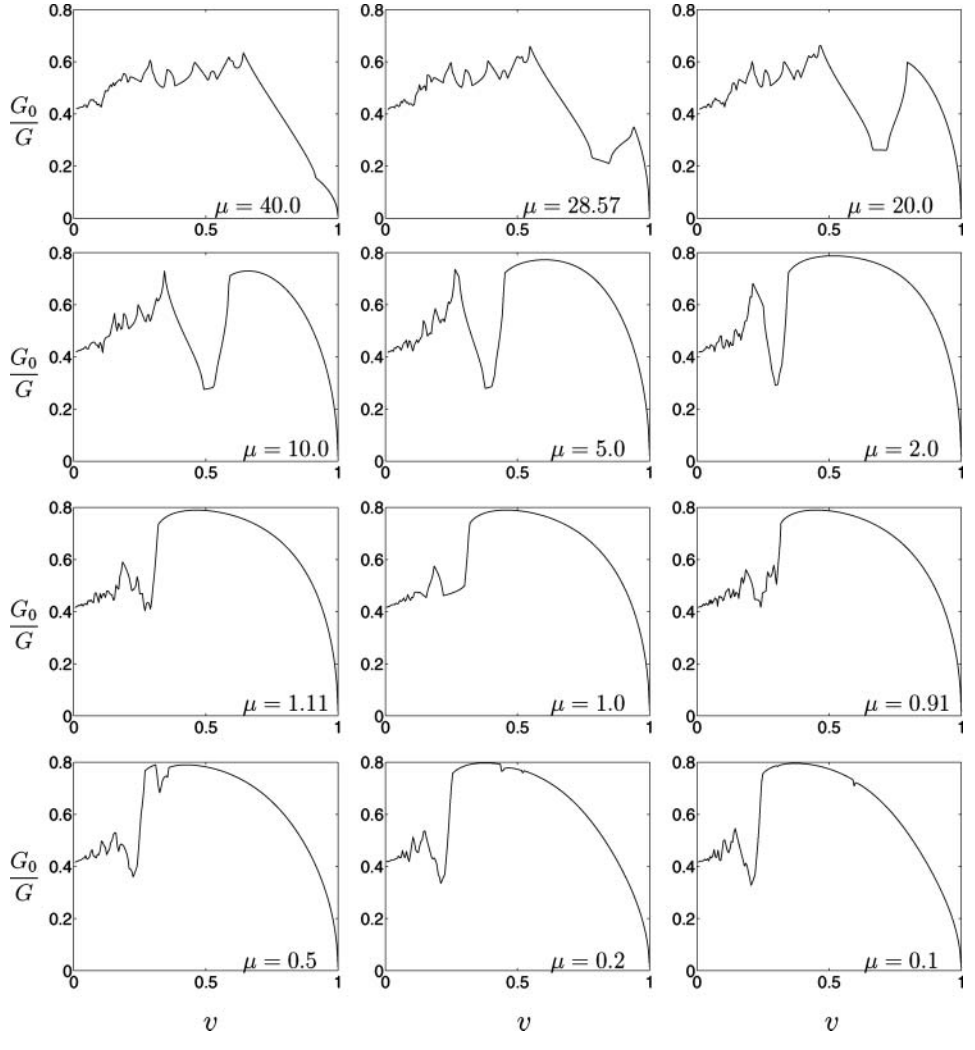

Figure 7. The energy ratio as a function of the crack speed v for different values of the lattice contrast parameter μ.

4.5 *Limiting case:* $\mu \to \infty$

In the limit $\mu \to \infty$, the black masses in figure 1(a) become zero, and only white masses remain. The kernel function $L(k)$ takes the asymptotic form

$$L(k) \sim \frac{5 - 2\cos(k)}{3 - 2\cos(k)} \quad \text{as} \quad k \to \infty, \tag{57}$$

and it does not tend to 1 at infinity.

To be able to apply the standard factorization algorithm, we introduce the normalized kernel function

$$\mathcal{L}(k) = L(k)/l(k), \quad \text{where} \quad l(k) = \frac{5 - 2\cos(k)}{3 - 2\cos(k)}, \tag{58}$$

and hence $\mathrm{Ind}(\mathcal{L}) = 0$ and $\mathcal{L}(k) \to 1$ as $k \to \pm\infty$.

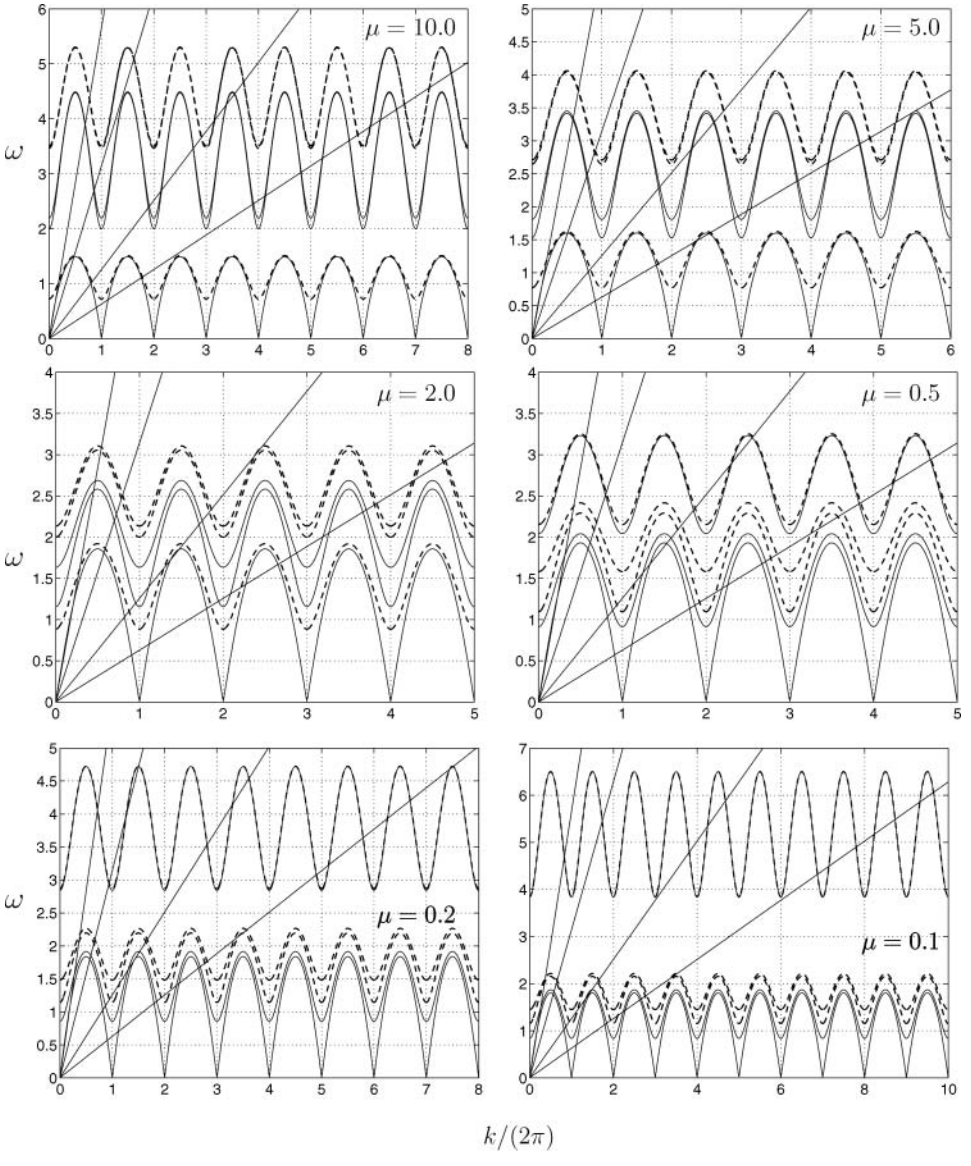

Figure 8. Dispersion diagrams with the rays $\omega = kv$, $v = 0.1$, 0.2, 0.5 and 0.9, for different values of the lattice contrast, μ.

Thus, factorizing in turn $\mathcal{L}(k)$ and $l(k)$ we obtain the required factorization of the kernel function $L(k)$. For the factorization in the form $\mathcal{L} = \mathcal{L}_+\mathcal{L}_-$, we can use the regular Cauchy-type integral. At the same time, the 2π-periodic function $l(k)$ can be factorized using the periodic version of the Cauchy-type integral

$$l_+(k) = \exp\left[\frac{1}{2\pi}\int_{-\pi}^{\pi}\frac{\ln l(\xi)}{1-\exp(-\mathrm{i}(\xi-k))}\,\mathrm{d}\xi\right] \quad (\Im k > 0)\,,$$

$$l_-(k) = \exp\left[\frac{1}{2\pi}\int_{-\pi}^{\pi}\frac{\ln l(\xi)\exp(\mathrm{i}(\xi-k))}{1-\exp(\mathrm{i}(\xi-k))}\,\mathrm{d}\xi\right] \quad (\Im k < 0). \tag{59}$$

The local energy release rate equal to the bond critical strain energy is

$$G_0 = \sigma(+0)u(+0) = 2\lim_{s\to\infty}(s^2)u_+(\mathrm{i}s)^2 = \frac{2C^2}{\mathcal{L}_+^2(\mathrm{i}\infty)l_+^2(\mathrm{i}\infty)} = 2C^2\alpha^2, \tag{60}$$

where

$$\alpha = \frac{1}{l_+(\mathrm{i}\infty)} = \exp\left[-\frac{1}{\pi}\int_0^\pi \ln\, l(k)\,\mathrm{d}k\right] = \frac{3+\sqrt{5}}{5+\sqrt{21}} \quad [\mathcal{L}_+(\mathrm{i}\infty) = 1]\,. \tag{61}$$

The global energy release rate relation (53) takes the form

$$G = \lim_{\varepsilon\to+0}\frac{2C^2\mathcal{L}_-(-\mathrm{i}\varepsilon)l_-(-\mathrm{i}\varepsilon)}{\mathcal{L}_+(\mathrm{i}\varepsilon)l_+(\mathrm{i}\varepsilon)}. \tag{62}$$

The use of the regular Cauchy-type integral leads to the following relation

$$\frac{\mathcal{L}_-(-\mathrm{i}0)}{\mathcal{L}_+(\mathrm{i}0)} = \mathcal{R}_{\mathcal{L}}^{-2} = \exp\left[-\frac{2}{\pi}\int_0^\infty \frac{\mathrm{Arg}\,\mathcal{L}(k)}{k}\,\mathrm{d}k\right]. \tag{63}$$

For $k \to 0$, each of the integrals in (59) can be represented as a sum of a half-residue at $\xi = 0$ and the principal value integral. Taking into account the symmetry, $l(-k) = l(k)$, we derive

$$\frac{l_-(-\mathrm{i}0)}{l_+(\mathrm{i}0)} = \exp\left[-\frac{1}{\pi}\int_0^\pi \ln l(k)dk\right] = \alpha. \tag{64}$$

Thus

$$G = \lim_{\varepsilon\to+0}\frac{2C^2L_-(-\mathrm{i}\varepsilon)}{L_+(\mathrm{i}\varepsilon)} = \frac{2C^2\alpha}{\mathcal{R}_{\mathcal{L}}^2(v)}, \tag{65}$$

and the energy ratio is equal to

$$\frac{G_0}{G} = \alpha\mathcal{R}_{\mathcal{L}}^2. \tag{66}$$

Note that $\mathrm{Arg}\,\mathcal{L} = \mathrm{Arg}\,L$ and hence $\mathcal{R}_{\mathcal{L}} = \mathcal{R}$. The lattice structure and the energy ratio for this limiting case are presented in figures 9(a) and 9(b), respectively.

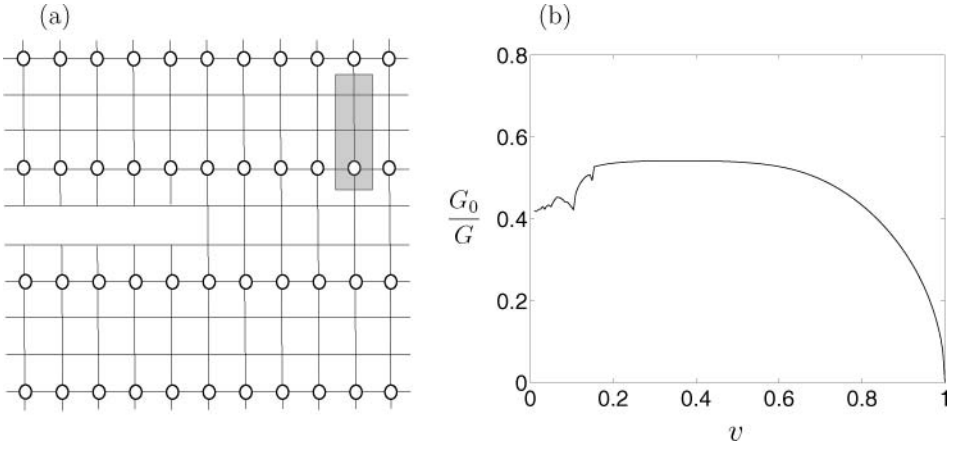

Figure 9. The limiting lattice structure, $\mu = \infty$, with one mass in the three-nod cell: (a) The lattice structure; (b) The energy ratio versus v.

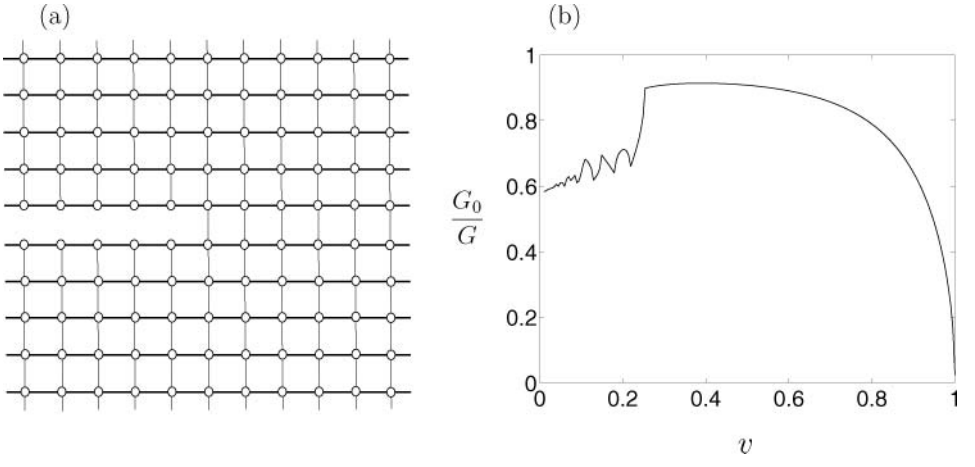

Figure 10. The orthotropic lattice: (a) The lattice structure, (b) The energy ratio versus v.

4.6 *Orthotropic lattice*

The above technique can be applied to a various lattice structures. The only essential condition is the uniformity in the crack propagation direction. Consider, for example, a lattice with an arbitrary stiffness, ν, of the 'vertical' bonds (see figure 10(a)). For simplicity the uniform mass distribution is assumed. The equation for the intact lattice is

$$\ddot{u}_{m,n} = u_{m-1,n} + u_{m+1,n} + \nu(u_{m,n-1} + u_{m,n+1}) - 2(1+\nu)u_{m,n} \tag{67}$$

with the dispersion relation

$$\omega^2 = 2(1+\nu) - 2\cos k_x - 2\nu\cos k_y. \tag{68}$$

For long waves

$$\omega^2 \sim k_x^2 + \nu k_y^2. \tag{69}$$

In terms of the Fourier transform on η, we get

$$u_n^F = u_0^F \lambda^n \tag{70}$$

with

$$\lambda = P_o - \sqrt{P_o^2 - 1}\,, \quad P_o = [1 + \nu + (0 + \mathrm{i}kv)^2/2 - \cos k]/\nu. \tag{71}$$

For the lattice with the crack the equation for $n = 0$ is

$$\ddot{u}_{m,0} = u_{m-1,0} + u_{m+1,0} + \nu(u_{m,1} - u_{m,0}) - 2(1+\nu)u_{m,0} + 2\nu u_{m,0}H(-\eta). \tag{72}$$

From this we find the Wiener–Hopf type equation (44) with

$$L(k) = \frac{2 + 3\nu + (0 + \mathrm{i}kv)^2 - 2\cos k - \nu\lambda}{2 + \nu + (0 + \mathrm{i}kv)^2 - 2\cos k - \nu\lambda}. \tag{73}$$

The energy ratio is defined by equations (56) and (52) with the above expression used for $L(k)$. For $\nu = 1/3$ it is presented as a function of the crack speed in figure 10(b).

5. Discussion

We have constructed the analytical solution for the dynamic fracture problem in an inhomogeneous lattice. The explicit connection between the crack resistance and the dispersion properties of the periodic lattice has been established and the total energy dissipation rate caused by waves excited in the lattice by the propagating crack has been determined. These waves correspond to those crack-speed-dependent regions of the k-axis (as the wavenumber axis) where $\lambda = \pm 1$ and where λ is complex (in this latter case, $|\lambda| = 1$ as well), that is, where $P^2 \leq 1$ [see (26)].

An interesting phenomenon revealed in this paper is a considerable *energy ratio drop-down* which arises in the energy ratio diagram for a certain region of the lattice contrast, μ (see figure 7). It mainly arises when $\mu > 1$, and the corresponding region on the v-axis moves to the right as μ increases (see the diagrams in figure 7 for $\mu = 2, 5, 10, 20$). With the further increase of μ, this *drop-down* approaches the critical crack speed where the energy ratio equals zero. The case $\mu = 10$ is presented in figure 11; also see figure 7. It is demonstrated in figure 11 that the *energy ratio drop-down* arises due to the highly increased region of the nonzero Arg $L(k)$ (see figure 11(c)) corresponding to the higher-order branches of the dispersion relation (figure 11(b)), that is, it corresponds to the increased dissipation caused by the higher-order-branch oscillations of the lattice particles.

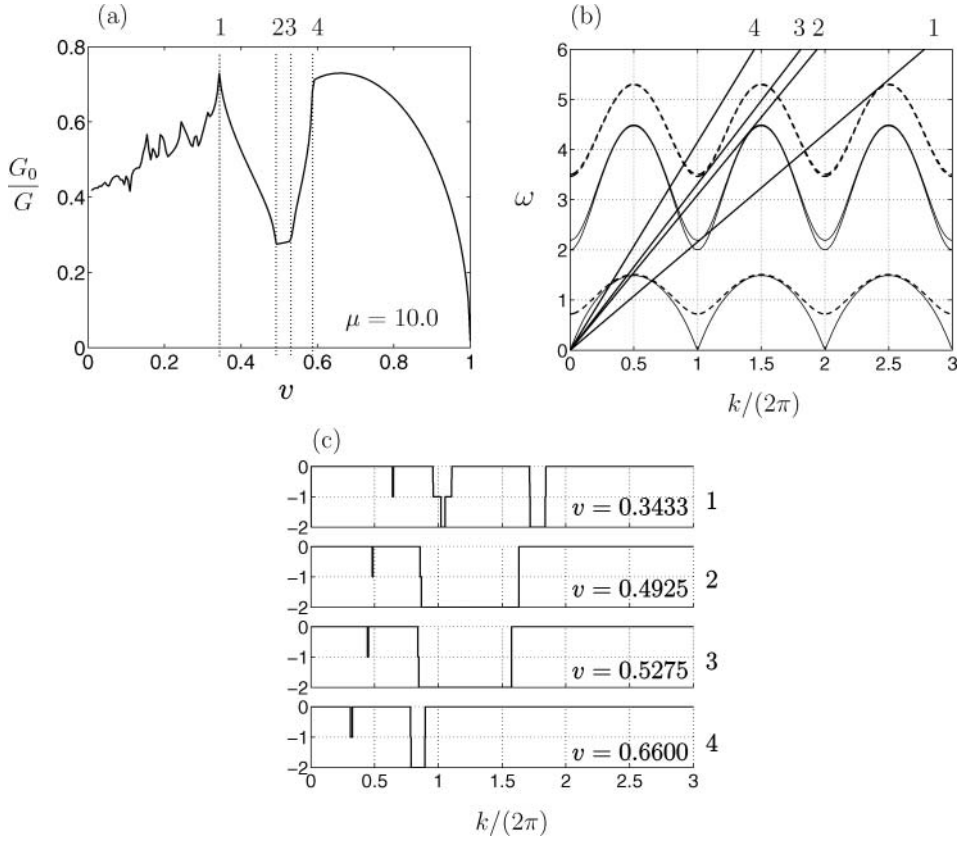

Figure 11. (a) The energy ratio for $\mu = 10$. The characteristic crack speeds, $v_1 < v_2 < v_3 < v_4$, for the *energy ratio drop-down* are marked by dotted vertical lines. (b) The corresponding dispersion curves together with the rays $\omega = kv_j$, $j = 1, 2, 3, 4$, (c) The normalized argument $2\pi^{-1}$ Arg$L(k)$ for the characteristic speeds.

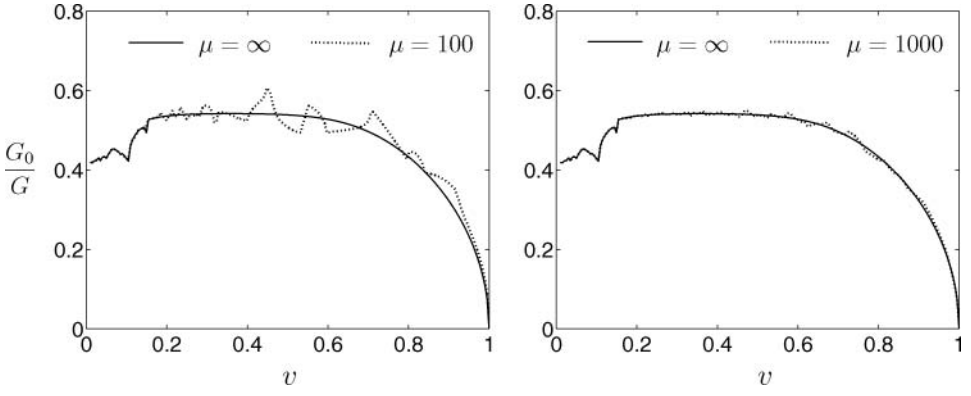

Figure 12. Comparison of the energy ratio for the limiting case ($\mu = \infty$, solid curves) and the pre-limiting case ($\mu = 100$ and $\mu = 1000$, dotted curves).

It is worth mentioning that for any small 'black' masses the higher-order branches exist with $\omega \to \infty$ as $\mu \to \infty$. For any finite μ the function $L(k) \to 1$ as $k \to \pm\infty$, and the higher-order oscillation modes still give a finite contribution to the dissipation. In the limiting case, $\mu = \infty$, there are no such branches; however, their contribution to the dissipation remains; it is reflected by the multiplier α in formula (66). This multiplier arises due to the adjustment in the factorization required for the case of a different asymptotic behavior of the Wiener–Hopf equation kernel $L(k)$ for $k \to \pm\infty$ when the 'black' masses disappear. We demonstrate in figure 12 how the results, corresponding to a finite μ, approach the limiting case as μ increases.

The *energy ratio drop-down* region corresponds to a highly increased dissipation, and hence to a strong increase of the crack resistance. Thus the above-mentioned increase in the lattice contrast μ creates an energy barrier against further increase of the crack speed. According to the results presented in figures 7 and 11 for the case of a crack in the inhomogeneous lattice with $2 < \mu < 10$, there exists a stability interval for sufficiently low crack speeds. We note that such an interval does not exist for a crack in a uniform lattice, as first noted in [18].

Acknowledgements

This paper was written during the academic visit of Prof. Slepyan to Liverpool University supported by the research grant EP/D079489/1 from the UK Engineering and Physical Sciences Research Council. Prof. Mishuris was supported by the Marie Curie Transfer of Knowledge Fellowship of the European Community's Sixth Framework Programme, grant reference MTKD-CT-2004-509809.

References

[1] Brillouin, L., 1953, *Wave Propagation in Periodic Structures* (NY: Dover).
[2] Maradudin, A. A., Montroll, E. W. and Weiss, G. H., 1963, *Theory of Lattice Dynamics in the Harmonic Approximation* (London: Academic Press).
[3] Yablonovitch, E., 1987, Inhibited spontaneous emission in solid-state physics and electronics. *Physical Review Letters*, **58**, 2059–2062.
[4] Yablonovitch, E., 1993, Photonic band-gap crystals. *Journal of Physics: Condensed Matter*, **5**, 2443–2460.
[5] John, S., 1987, Strong localization of photons in certain disordered dielectric superlattices. *Physical Review Letters*, **58**, 2486–2489.

[6] Joannopoulos, J. D., Meade, R. D. and Winn, J.N., 1995, *Photonic Crystals: Molding the Flow of Light* (Princeton, NJ: Princeton University Press).

[7] Johnson, S. G. and Joannopoulos, J. D., 2002, *Photonic Crystals. The Road from Theory to Practice* (Boston: Kluwer Acad. Publ.).

[8] Gorishnyy, T., Ullal, C. K., Maldovan, M., Fytas, G. and Thomas, E. L., 2005, Hypersonic phononic crystals. *Physical Review Letters*, **94**, 115–501.

[9] Thomson, R., Hsieh, C. and Rana, V., 1971, Lattice trapping of fracture cracks. *Journal of Applied Physics*, **42**, 3154–3160. (DOI:10.1063/1.1660699)

[10] Ashurst, W. T. and Hoover, W. G., 1976, Microscopic fracture studies in the two-dimensional triangular lattice. *Physical Review B*, **14**, 1465–1473.

[11] Wang, Yu., Abe, S., Latham, S. and Mora, P., 2004, Implementation of particle-scale rotation in the 3-D lattice solid model. http://www.aces-workshop-2004.ac.cn/html/fullpaper/wangyucang.doc

[12] Zhu, B. T., Li, Y. and Yip, S., 2006, Atomistic characterization of three-dimensional lattice trapping barriers to brittle fracture. *Proceedings of the Physical Society Section A*, **462**, 1741–1761. (DOI:10.1098/rspa.2005.1567).

[13] Slepyan, L. I., 1981, Dynamics of a crack in a lattice. *Soviet Physics Doklady*, **26**, 538–540.

[14] Kulakhmetova, S. A., Saraikin, V. A. and Slepyan, L., 1984, Plane problem of a crack in a lattice. *Mechanics of Solids*, **19**, 101–108.

[15] Fineberg, J., Gross, S. P., Marder, M. and Swinney, H. L., 1991, Instability in dynamic fracture. *Physical Review Letters*, **67**, 457–460.

[16] Fineberg, J., Gross, S. P., Marder, M. and Swinney, H. L., 1992, Instability in the propagation of fast cracks. *Physical Review B*, **45**, 5146–5154.

[17] Marder, M. and Liu, X, 1994, Instability in lattice fracture. *Physical Review E*, **50**, 188–197.

[18] Marder, M. and Gross, S., 1995, Origin of crack tip instabilities. *Journal of the Mechanics and Physics of Solids*, **43**, 1–48.

[19] Marder, M. and Fineberg, J., 1996, How things break. *Physics Today*, **49**, 1–12.

[20] Kessler, D. A., 1999, Arrested cracks in nonlinear lattice models of brittle fracture. *Physical Review E*, **60**, 7569–7571.

[21] Kessler, D. A., 2000, Steady-state cracks in viscoelastic lattice models. II. *Physical Review E*, **61**, 2348–2360.

[22] Fineberg, J. and Marder, M., 1999, Instability in dynamic fracture. *Physical Reports*, **313**, 1–108.

[23] Kessler, D. A. and Levine, H., 2001, Nonlinear lattice model of viscoelastic mode III fracture. *Physical Review E*, **63**, 016118.

[24] Kessler, D. A. and Levine, H., 2003, Does the continuum theory of dynamic fracture work? *Physical Review E*, **68**, 036118.

[25] Slepyan, L. I., 2001, Feeding and dissipative waves in fracture and phase transition. I. Some 1D structures and a square-cell lattice. *Journal of the Mechanics and Physics of Solids*, **49**, 25–67.

[26] Slepyan, L. I., 2001, Feeding and dissipative waves in fracture and phase transition. III. Triangular-cell lattice. *Journal of the Mechanics and Physics of Solids*, **49**, 2839–2875.

[27] Slepyan, L. I., 2005, Crack in a material-bond lattice. *Journal of the Mechanics and Physics of Solids*, **53**, 1295–1313.

[28] Heizler, S. I., Kessler, D. A. and Levine, H., 2002, Mode-I fracture in a nonlinear lattice with viscoelastic forces. *Physical Review E*, **66**, 016126.

[29] Slepyan, L. I. and Ayzenberg-Stepanenko, M. V., 2002, Some surprising phenomena in weak-bond fracture of a triangular lattice. *Journal of the Mechanics and Physics of Solids*, **50**, 1591–1625.

[30] Slepyan, L. I. and Ayzenberg-Stepanenko, M. V., 2004, Localized transition waves in bistable-bond lattices. *Journal of the Mechanics and Physics of Solids*, **52**, 1447–1479.

[31] Slepyan, L. I. and Ayzenberg-Stepanenko, M. V., 2006, Crack dynamics in nonlinear lattices. *International Journal of Fracture*, **140**, 235–242.

[32] Slepyan, L. I., 2002, *Models and Phenomena in Fracture Mechanics* (Berlin: Springer).

[33] Herrmann, H. J., Hansen, A. and Roux S., 1989, Fracture of disordered, elastic lattices in two dimensions. *Physical Review B*, **39**, 637–648.

[34] Tzschichholz, F., Herrmann, H. J., Roman, H. E. and Pfuff, M., 1994, Beam model for hydraulic fracturing. *Physical Review B*, **49**, 7056–7059.

[35] Chen, J. Y., Huang, Y. and Ortiz, M., 1998, Fracture analysis of cellular materials. *Journal of the Mechanics and Physics of Solids*, **46**, 789–828.

[36] Astrom, J. and Timonen, J., 1996, Crack bifurcation in a strained lattice. *Physical Review B*, **54**, 9585–9588.

[37] Gibson, L. J. and Ashby, M. F., 1997, *Cellular solids - structure and properties*, 2nd edn. (Cambridge: Cambridge University Press).

[38] Schmidt, I. and Fleck, N. A., 2001, Ductile fracture of two-dimensional cellular structures. *International Journal of Fracture*, **111**, 327–342.

[39] Skjetne, B., Helle, T. and Hansen, A., 2005, Brittle crack roughness in three-dimensional beam lattices. arXiv: cond-mat/0505633v1, 1–4.

[40] Lipperman, F., Ryvkin, M. and Fuchs, M. B., 2005, Nucleation of cracks in two-dimensional periodic cellular materials. *Computational Mechanics* (DOI 10.1007/s00466-005-0014-9)

[41] Slepyan, L. I., 2000, Dynamic factor in impact, phase transition and fracture. *Journal of the Mechanics and Physics of Solids*, **48**, 927–960.